Available online at www.sciencedirect.com

ScienceDirect

Ceramics International 40 (2014) 2877–2884

CERAMICS INTERNATIONAL

www.elsevier.com/locate/ceramint

Microwave-hydrothermal synthesis of Fe-based materials for lithium-ion batteries and supercapacitors

Kunfeng Chen[a], Young Dong Noh[b], Wenyan Huang[b,c], Jianfeng Ma[b,d], Sridhar Komarneni[b,*], Dongfeng Xue[a,*]

[a]State Key Laboratory of Rare Earth Resource Utilization, Changchun Institute of Applied Chemistry, Chinese Academy of Sciences, Changchun 130022, China

[b]Materials Research Institute, Materials Research Laboratory, The Pennsylvania State University, University Park, PA 16802, USA

[c]School of Materials Science and Engineering, Changzhou University, Changzhou 213164, China

[d]School of Environmental and Safety Engineering, Changzhou University, Changzhou 213164, Jiangsu, China

Received 30 September 2013; received in revised form 6 October 2013; accepted 6 October 2013
Available online 11 October 2013

Abstract

Fe-based materials, Fe_2O_3, Fe_3O_4, and FeOOH, were synthesized by the microwave–hydrothermal process in the temperature range of 100–200 °C and under very short reaction times of 15 min to 2 h. Under microwave-controlled hydrolysis and redox reactions, cube-like Fe_2O_3 was crystallized using $FeCl_3$, Fe_3O_4 particles were crystallized from $FeCl_2$ and FeOOH nanorods were crystallized using $FeCl_3$. The Fe-based materials were fabricated to make anodes and cathodes of lithium-ion battery and supercapacitor electrode materials to study their potential electrochemical applications. The electrochemical results showed that FeOOH had better anode capacity as lithium-ion batteries than those of Fe_2O_3 and Fe_3O_4. The present results suggest that the microwave–hydrothermally synthesized Fe-based materials are promising lithium-ion battery anode materials.

Keywords: Fe_2O_3; Fe_3O_4; FeOOH; Lithium-ion battery; Supercapacitor

1. Introduction

Materials synthesis and processing by environmentally benign or green chemical approaches using earth abundant materials is one of the keys to reduce environmental damage and energy consumption [1–4]. The microwave-assisted and microwave–hydrothermal processes have been touted as greener, faster, cheaper and better than conventional methods for materials synthesis starting as early as 1985 by Komarneni's group [5–7]. Materials synthesis obviously is the initial process to study the performance of as-obtained materials with a good understanding of the chemical properties of materials, reaction reagents and solvents [8–10]. In addition, the performances and functions of materials can be controlled by inherent properties, such as band gap, hardness, crystal structure, and electronegativity etc. [11–15]. Iron (Fe) is an important earth abundant chemical element and commonly exists as +2 and +3 oxidation states in solution. The common iron–oxygen compounds are Fe_2O_3, FeOOH, Fe_3O_4 and FeO. Fe-based materials can be synthesized by controlling the valence state of the soluble iron salts of Fe^{3+} and Fe^{2+} ions in solid or solution phases. For example, Mn-based materials of different phases, structures and sizes have been formed by controlling the chemical reactions of Mn^{2+} and Mn^{7+} [16–19]. The chemical reaction controlled synthesis is a promising and powerful route to crystallize transition metal oxide nano/micromaterials [20–22].

Iron oxides are potential electrode materials as lithium-ion batteries and supercapacitors owing to their low cost and low toxicity [23,24]. Various synthesis methods have been used to grow iron oxides with different structures, phase, and sizes, and their electrochemical performances have been evaluated as

*Corresponding authors.
E-mail addresses: komarneni@psu.edu (S. Komarneni), dongfeng@ciac.ac.cn (D. Xue).

0272-8842/$ - see front matter © 2013 Elsevier Ltd and Techna Group S.r.l. All rights reserved.
http://dx.doi.org/10.1016/j.ceramint.2013.10.024

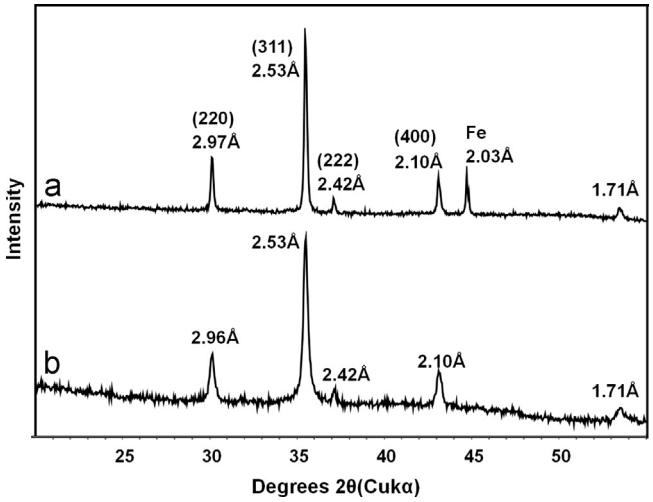

Fig. 1. XRD patterns of (a) magnetite, Fe_3O_4 and trace amount of Fe metal prepared at 150 °C/15 min and (b) Fe_3O_4 prepared at 100 °C/15 min using the M–H process.

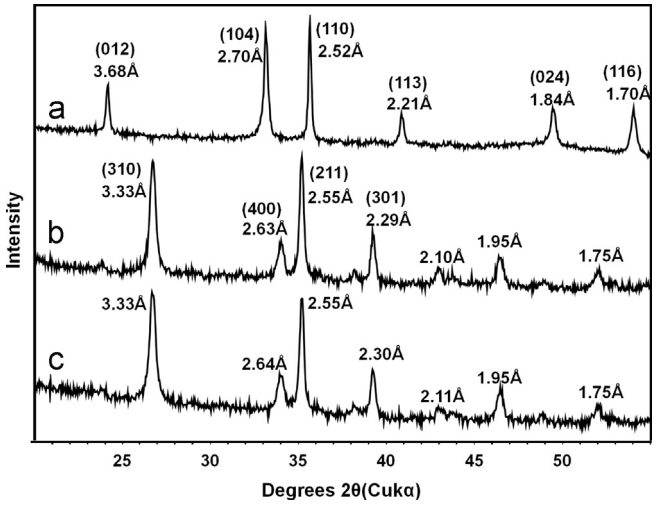

Fig. 2. XRD patterns of (a) hematite, Fe_2O_3 prepared at 150 °C/2 h, (b) akaganeite, FeOOH prepared at 125 °C/2 h and (c) akaganeite, FeOOH prepared at 100 °C/2 h using the M–H process.

electrode materials. The microwave–hydrothermal process is potentially advantageous for the synthesis of iron oxide materials because it can dramatically reduce the reaction time from several hours or even days down to 30 min while controlling the morphology to produce narrow size distribution of particles with high purity [5–7]. Recently, We reported microwave – hydrothermal process to crystallize polymorphs of MnO_2 such as α-, β-, and γ-phase samples with the plate-, rod-, and wire-like shapes by controlling the oxidation–reduction reactions in $MnCl_2$–$KMnO_4$ aqueous solution system [7].

Herein, we report the synthesis of Fe-based oxide materials of Fe_2O_3, Fe_3O_4, and FeOOH by the microwave–hydrothermal process using short reaction times (15 min to 2 h). Cube-like Fe_2O_3, FeOOH nanorods and Fe_3O_4 particles were crystallized by the controllable hydrolysis and redox reactions of $FeCl_3$ or $FeCl_2$. The Fe-based materials were processed to make anodes and cathodes of lithium-ion battery and supercapacitor to study their potential electrochemical applications. The electrochemical measurement results showed that FeOOH had better anodes capacity as lithium-ion battery than that of either Fe_2O_3 or Fe_3O_4. The microwave–hydrothermally synthesized Fe-based materials are shown below as promising lithium-ion battery anode and supercapacitor materials.

2. Experimental

2.1. Synthesis

One Fe_2O_3 (hematite) sample was synthesized by the microwave–hydrothermal (M–H) process at 150 °C for 2 h using 0.09 M $FeCl_3$ solution in 0.01 M HCl. Two FeOOH (akaganeite) samples were prepared using the M–H process at 100 °C or 125 °C for 2 h using 0.09 M $FeCl_3$ solution in 0.01 M HCl. Two Fe_3O_4 (magnetite) samples were also prepared using the M–H process as follows: 0.016 mol of $FeCl_2$ was dissolved in 25 ml of ethanol in a Teflon vessel.

Table 1
Capacities of obtained products as lithium-ion battery anodes.

Sample no.	Phase	Microwave–hydrothermal condition	Anode capacity (mAh/g)				
			1st	2nd	10th	20th	30th
1	Fe_3O_4	150 °C 15 min	1136.2	666.8	153.7	98.6	76.2
2	Fe_3O_4	100 °C 15 min	1056.4	1008.6	163.7	78.6	53.7
3	Fe_2O_3	150 °C 2 h	1063.2	725.8	158.8	105.4	81.8
4	FeOOH	125 °C 2 h	243.9	446.7	178.3	233.6	182.1
5	FeOOH	100 °C 2 h	1328.3	757.8	321.5	208.8	163.4

Then 0.064 mol of NaOH was dissolved in 10 ml of deionized water. Under stirring, the NaOH solution was added to the $FeCl_2$ solution. The precursor was treated at 100 °C or 125 °C for 15 min under the M–H method [25]. The resultant solid reaction products were collected and washed several times with deionized water and ethanol to remove any soluble species by centrifugation. MARS-5 equipment was used to conduct the microwave–hydrothermal experiments in Teflon vessels. The temperature of treatment was precisely measured by an optical probe.

2.2. Characterization

The prepared samples were characterized by powder X-ray diffraction (XRD) for phase detection. Powder XRD patterns were obtained on a PANalyticalX'Pert MPD diffractometer operated at 45 kV voltage and 40 mA current with a PIXcel detector and using Cu Kα radiation. Field-emission scanning electron microscope (FESEM, Hitachi-S4800) was used to determine the particle size and shape of synthesized materials.

2.3. Lithium-ion battery

The working electrodes were prepared by mixing each active material, acetyleneblack, and polyvinylidene fluoride (PVDF) in

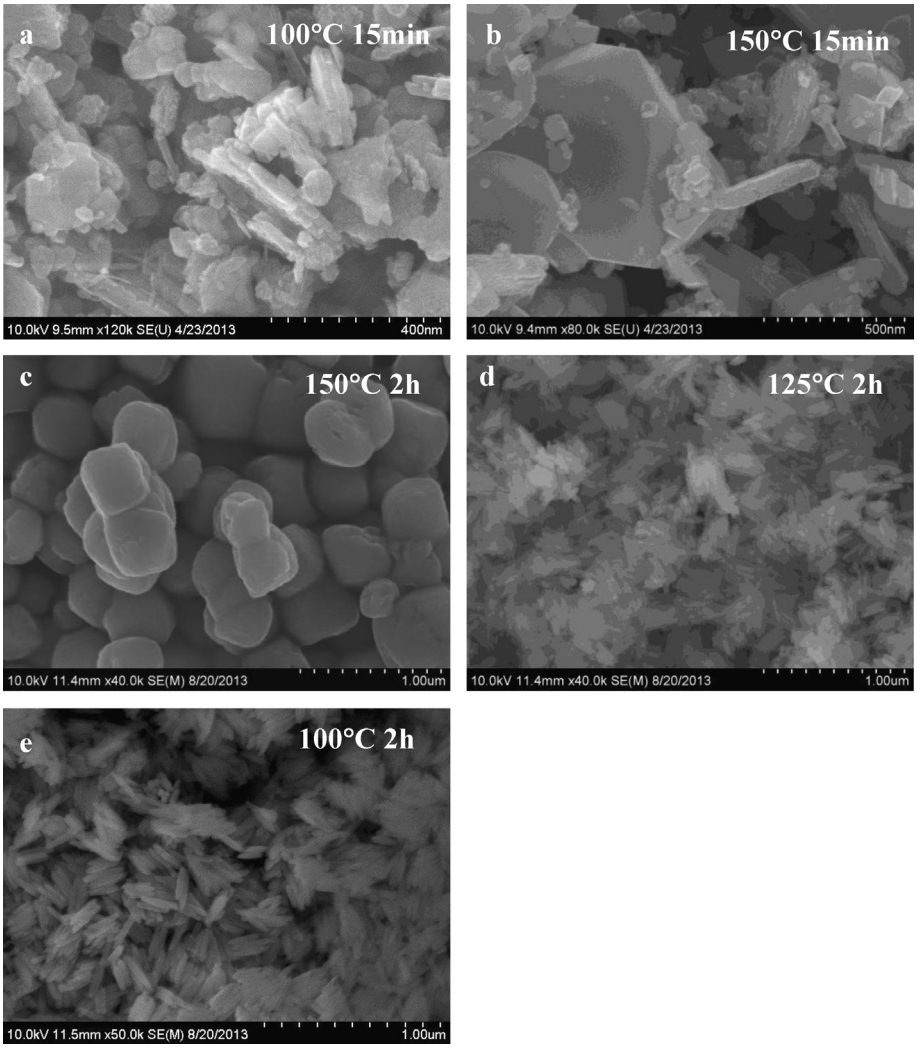

Fig.3. SEM images of as-obtained Fe-based products under M–H conditions. (a and b) Fe_3O_4, (c) Fe_2O_3, (d and e) FeOOH.

a weight ratio of 80:10:10. The mixtures were slurried with N-methyl-2-pyrrolidone, and pasted onto aluminum foil as cathodes and copper foil as anodes. The typical loading weight of active materials on each electrode is about 2–3 mg. For the electrochemical properties, coin cells (CR2025) were fabricated using lithium metal as the counter and reference electrodes. 1 M $LiPF_6$ in ethylene carbonate/dimethyl carbonate/diethyl carbonate (EC/DMC/DEC, 1:1:1 vol%) served as the electrolyte. A galvanostatic cycling test of the assembled half-cells was conducted on a LAND CT2001A system.

2.4. Supercapacitors

Working electrodes were prepared by pressing a mixture of each sample, acetylene black, and polyvinylidene fluoride (PVDF) in a weight ratio of 80:10:10 on porous nickel foil. The typical loading weight of active materials on each electrode is about 1–2 mg. All experiments were performed in a three-electrode open beaker cell in 1 M $LiNO_3$ or 1 M Li_2SO_4 under normal atmosphere. The samples/nickel foam was used as the working electrode, saturated calomelelectrode (SCE) as the reference electrode, and the Pt wire as a counter electrode. The cyclic voltammetry (CV), and galvanostatic charge–discharge measurements were carried out by an electrochemical workstation (CHI 660D).

3. Results and discussion

The XRD patterns of the as-obtained products after the M–H synthesis are shown in Figs. 1 and 2. Fig. 1 shows well crystallized magnetite (Fe_3O_4) at 100°C as well as 150 °C after the M–H treatment for just 15 min (Table 1). Hematite (Fe_2O_3) was crystallized at 150 °C after the M–H treatment for 2 h (Fig. 2, Table 1). Akaganeite (FeOOH) was crystallized at 100 °C as well as 125 °C after the M–H treatment for 2 h (Fig. 2, Table 1).

Fig. 3 shows SEM images of as-obtained Fe_3O_4, Fe_2O_3 and FeOOH. Fig. 3a shows that the less crystallized Fe_3O_4 particles at 100 °C for 15 min have different sizes and poorly developed faces while the well crystallized Fe_3O_4 particles at 150 °C for 15 min have different sizes and well-developed faces (Fig. 3b). Fe_2O_3 crystals were synthesized by the M–H route at 150 °C

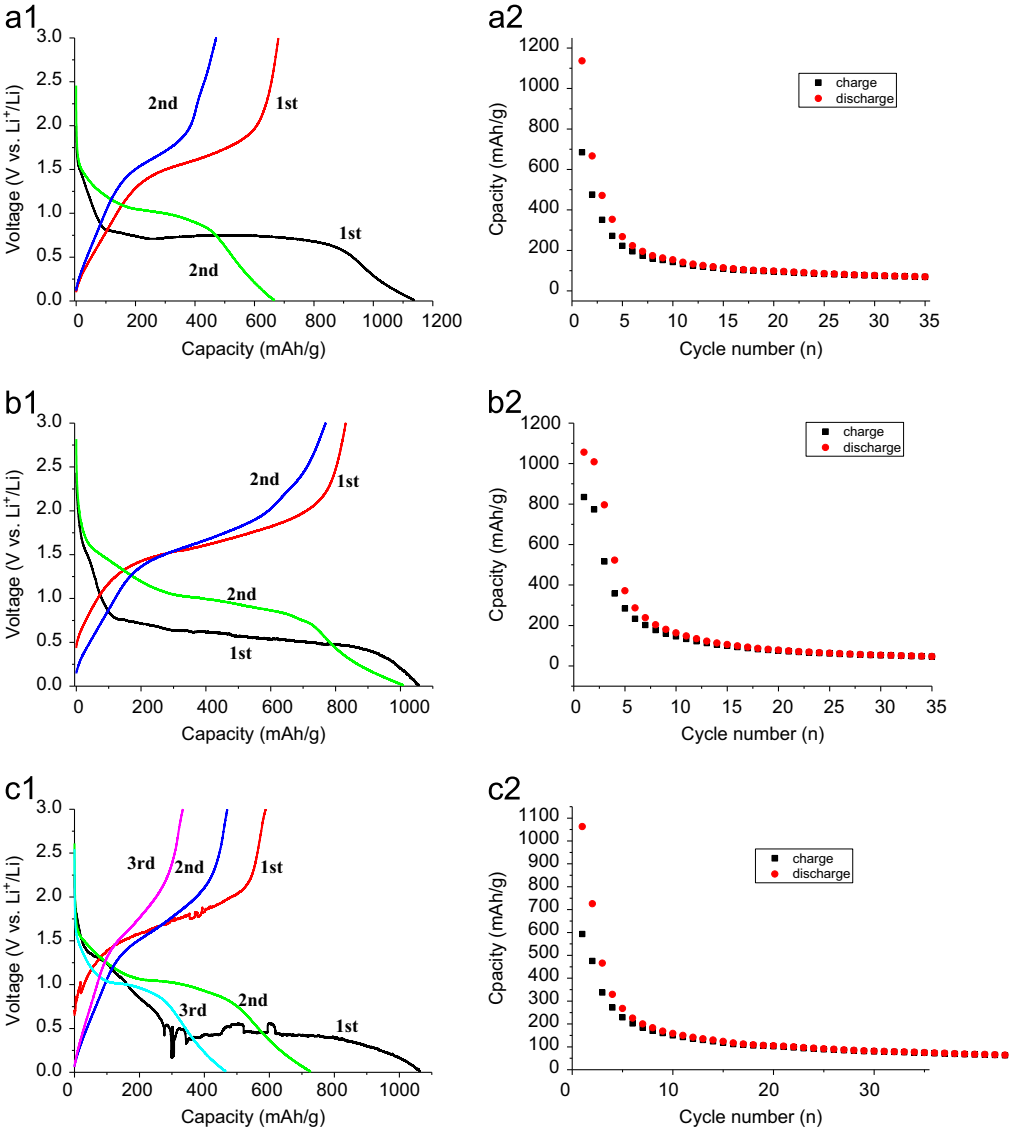

Fig. 4. Galvanostatic charge–discharge curves and cycling performances of Fe-based materials as lithium-ion battery anodes at current density of 100 mA/g. (a) Fe_3O_4 prepared at 150 °C/15 min, (b) Fe_3O_4 prepared at 100 °C/15 min, (c) Fe_2O_3 prepared at 150 °C/2 h.

for 2 h, and they have regular cube-like structures. FeOOH crystals were synthesized by the M–H route at 100 and 125 °C for 2 h, and both of them have nanorod morphologies.

To test their applicability, the electrochemical performances of lithium-ion batteries and supercapacitors were evaluated. The electrochemical performances of Fe-based materials as lithium-ion battery anodes are shown in Figs. 4 and 5 and Table 1. Figs. 4 and 5 show galvanostatic charge–discharge curves and cycling performances of Fe-based materials as lithium-ion battery anodes at a current density of 100 mA/g. The first discharge potential plateaus of Fe_3O_4 and Fe_2O_3 are less than 1 V (vs. Li^+/Li), while the second discharge potential plateaus are larger than 1 V. The discharge potential plateau indicated the conversion reaction of Fe-based electrode between iron oxide and metal Fe. The rise of redox potentials after the first lithiation is attributed to an increase in kinetics, which is due to the decrease in particle size of iron oxides. Fe_3O_4 and Fe_2O_3 showed similar charge–discharge curves, which indicated similar conversion reaction. The conversion reactions of Fe_3O_4 and Fe_2O_3 materials occurred during electrochemical processes, which can be represented as following equations:

$$Fe_2O_3 + 6Li^+ + 6e^- \rightarrow 2Fe + 3Li_2O \quad (1)$$

$$Fe_3O_4 + 8Li^+ + 8e^- \rightarrow 3Fe + 4Li_2O \quad (2)$$

FeOOH electrodes show different discharge potential plateaus, which suggested that the conversion reaction of FeOOH was different. The long voltage plateau of the first discharge curve at 0.5 V corresponds to the reduction of Fe^{3+} to Fe. The small plateau at 1.5 V in the first cycle can be attributed to the lithium intercalation before reduction reaction. FeOOH is reduced into nanoparticles of metallic Fe embedded in the amorphous matrix of Li_2O and LiOH in the first discharge. The subsequent cyclings are redox reactions between metallic Fe and Fe_2O_3 clusters [26].

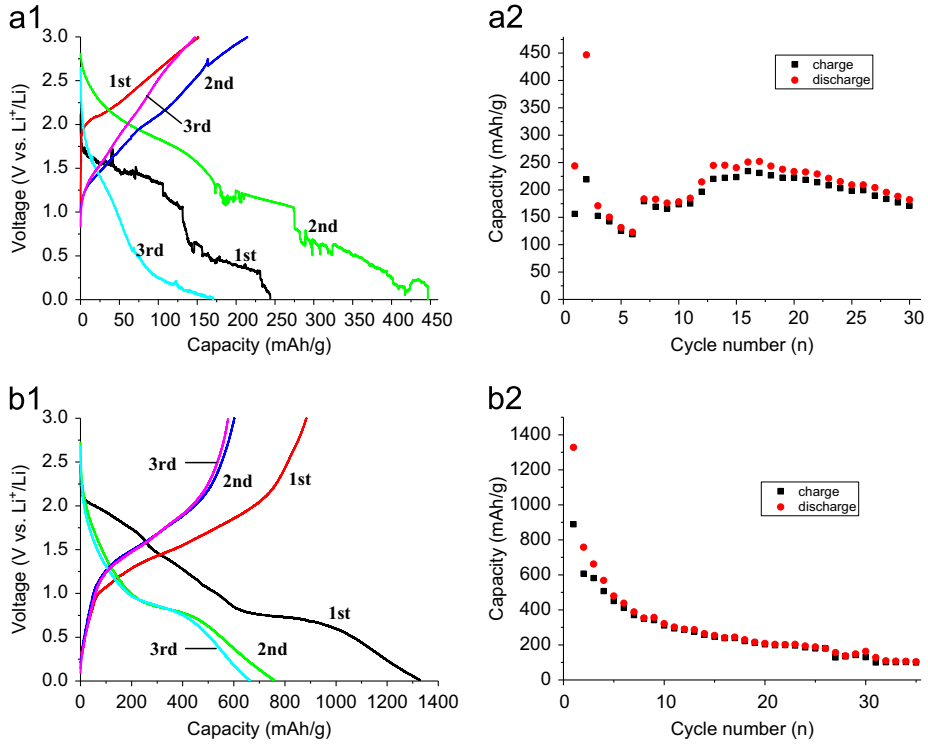

Fig. 5. Galvanostatic charge–discharge curves and cycling performances of FeOOH samples as lithium-ion battery anodes at current density of 100 mA/g. (a) FeOOH prepared at 125 °C/2 h, and (b) FeOOH prepared at 100 °C/2 h.

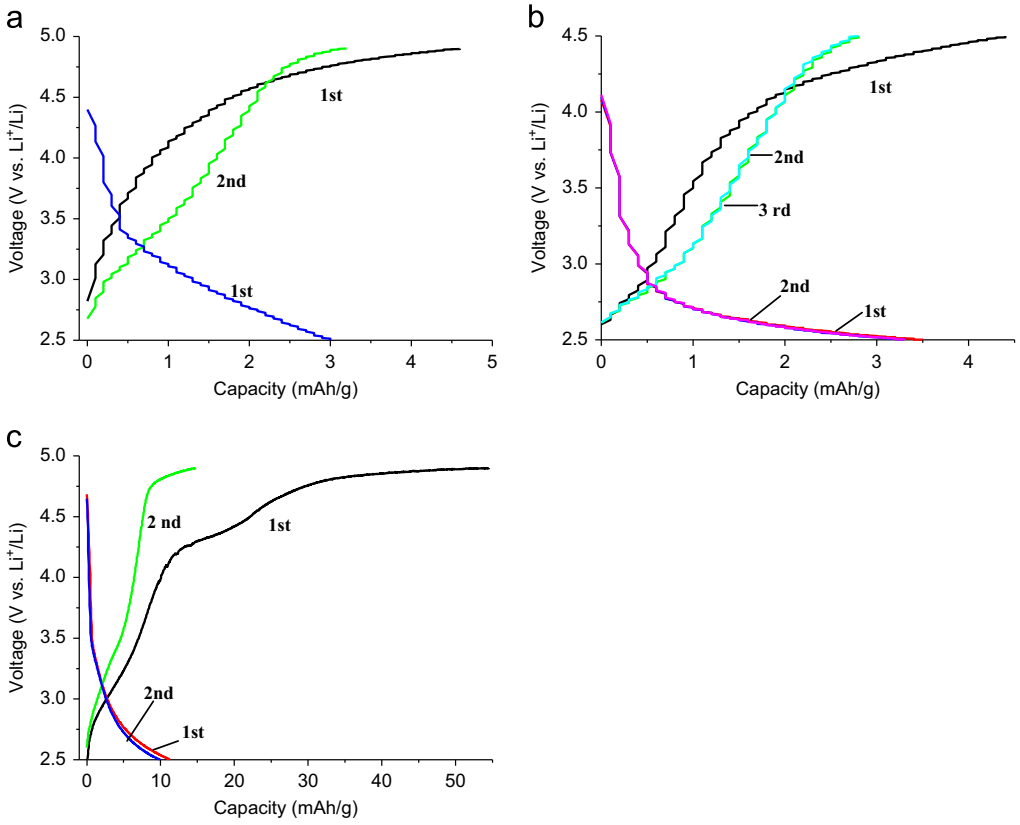

Fig. 6. Galvanostatic charge–discharge curves of Fe-based samples as lithium-ion battery cathodes at current density of 50 mA/g. (a) Fe_2O_3 prepared at 150 °C/2 h, (a) FeOOH prepared at 125 °C/2 h, (b) FeOOH prepared at 100 °C/2 h.

1st discharge process

$$FeOOH + 3Li^+ + 3e^- \rightarrow Fe + Li_2O + LiOH \quad (3)$$

Subsequent cycling

$$2Fe + 3Li_2O \leftrightarrow Fe_2O_3 + 6Li^+ + 6e^- \quad (4)$$

It should be noted that a large capacity loss existed in all Fe-based electrodes. The occurrence of irreversible redox reaction was probably the cause for the above large capacity loss [26–28]. The capacity of FeOOH is larger than those of Fe_3O_4 and Fe_2O_3 electrodes. In this reaction system, the morphology of FeOOH is 1D nanorod structure, which can favor the transfer of Li^+ and electron within 1D path during electrochemical reactions. Therefore, FeOOH electrodes can show better capacity and cycling stability (Fig. 5 and Table 1).

Table 2
Capacities of obtained products as lithium-ion battery cathodes.

Sample no.	Cathode capacity (mAh/g)				
	1st	2nd	10th	20th	30th
1	1	0.9	0.7	0.7	0.7
2	1.6	1.4	1.2	1.2	1.1
3	2.8	3	3.3	3.3	3.2
4	3.5	3.3	4.8	–	–
5	11.2	9.9	8.2	7.8	7.7

Fe-based materials were also used as lithium-ion battery cathodes and their electrochemical performances are shown in Fig. 6 and Table 2. The capacities of Fe-based materials were less than 10 mAh/g. The capacity of FeOOH as lithium-ion battery cathodes was larger than those of Fe_3O_4 or Fe_2O_3 electrodes. These results prove that the as-synthesized Fe_3O_4, Fe_2O_3 and FeOOH materials cannot show electrochemically high activity at potential range of 3–4.5 V (vs. Li^+/Li).

Furthermore, the electrochemical performances of Fe_3O_4, Fe_2O_3 and FeOOH materials were measured as supercapacitors in 1 M Li_2SO_4 or $LiNO_3$ electrolyte. Figs. 7 and 8 show CV curves at the scan rate of 10 mV/s and galvanostatic charge–discharge curves at the current density of 1 A/g of Fe-based materials. CV curves exhibited redox peaks, which indicated the pseudocapacitance of Fe-based materials. The value of the specific capacitance was obtained from the charge–discharge cycling measurements according to the following equation [7]:

$$SC = \frac{I\Delta t}{m\Delta E} \quad (5)$$

where I is the current used for charge/discharge in A, Δt is the time elapsed for the discharge cycle in s, m is the mass of the active electrode material in g, and ΔE is the voltage interval of the charge or discharge in V. The specific capacitances of Fe-based materials are shown in Table 3. The FeOOH electrodes showed the highest value of 14 F/g. FeOOH electrodes showed better electrochemical performance as lithium-ion battery

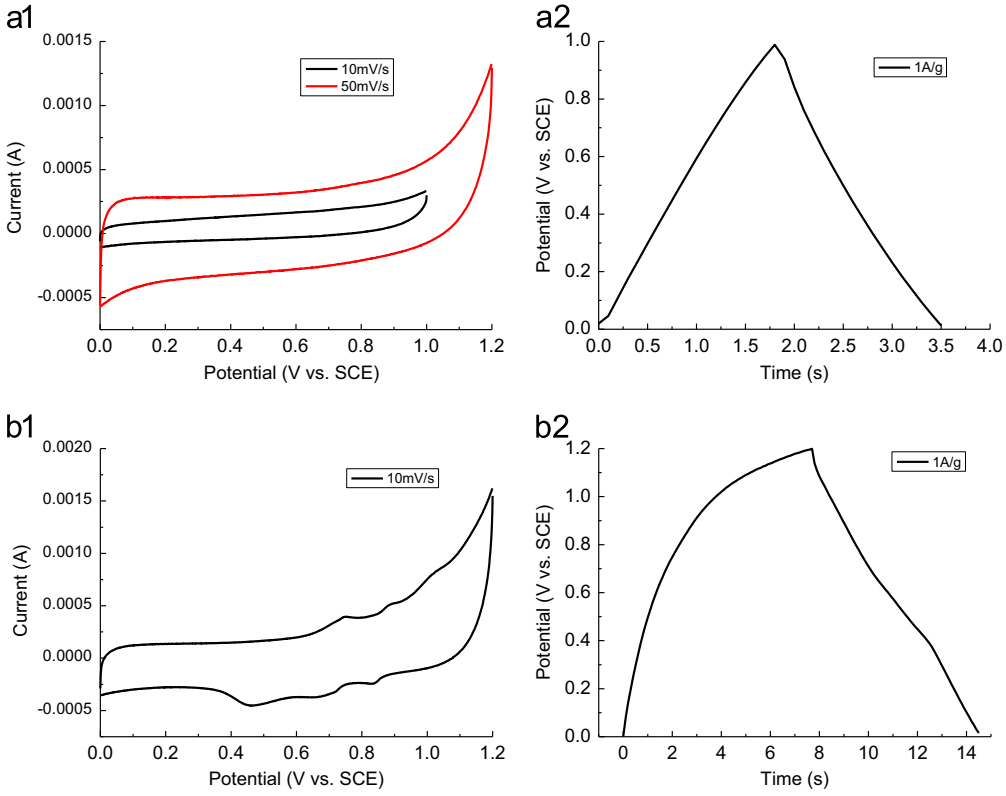

Fig. 7. CV curves at the scan rate of 10 mV/s and galvanostatic charge–discharge curves at the current density of 1 A/g of samples as supercapacitors in 1 M $LiNO_3$. (a) Fe_3O_4 prepared at 150 °C/15 min, and (b) Fe_3O_4 prepared at 100 °C/15 min.

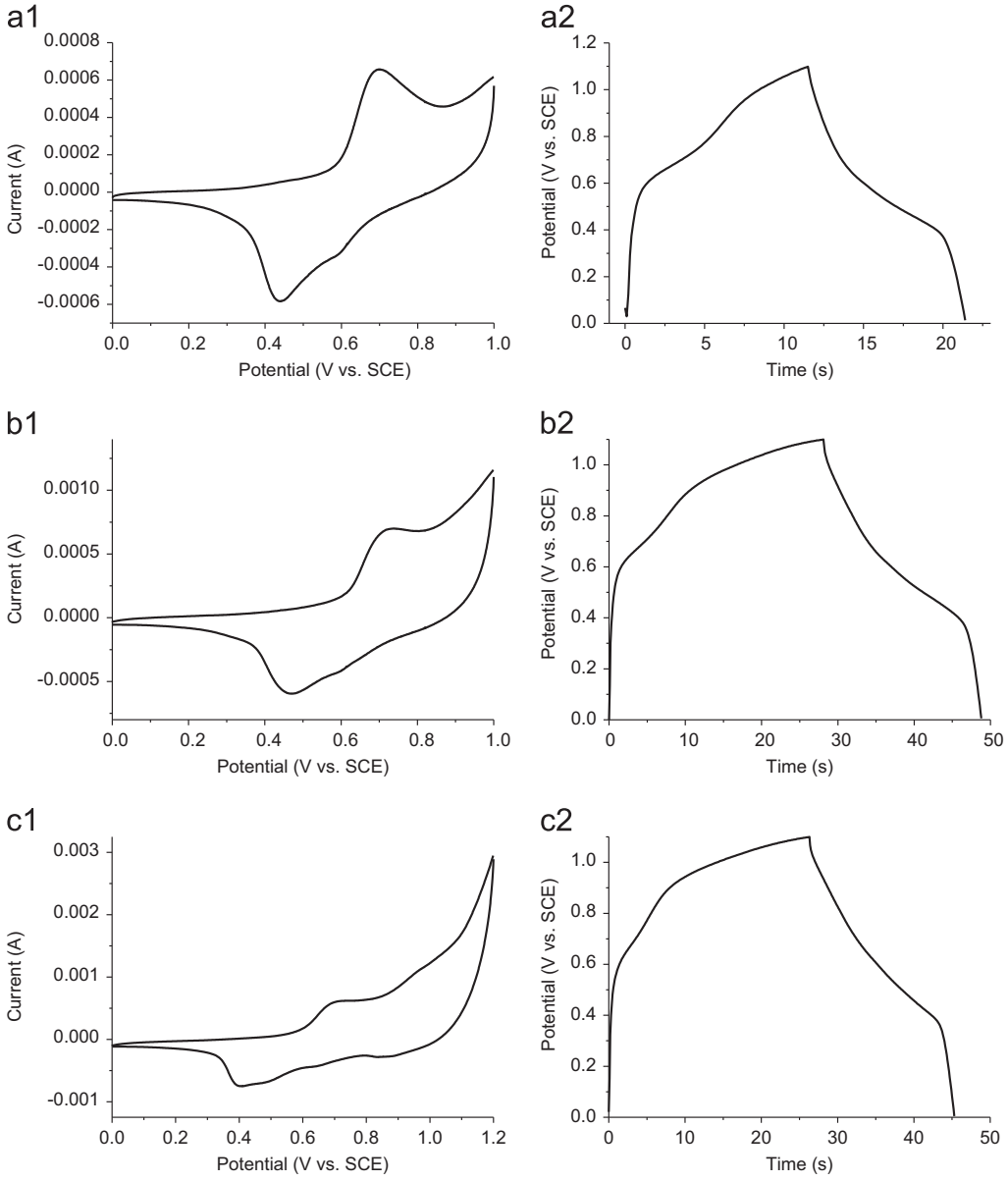

Fig. 8. CV curves at the scan rate of 10 mV/s and galvanostatic charge–discharge curves at the current density of 1 A/g of samples as supercapacitors in 1 M Li_2SO_4. (a) Fe_2O_3 prepared at 150 °C/2 h, (b) FeOOH prepared at 125 °C/2 h and (c) FeOOH prepared at 100 °C/2 h using the M–H process.

anode, cathode and supercapacitors than those of Fe_2O_3 and Fe_3O_4. This is probably because of FeOOH nanorod morphology, which can favor the electrochemical reactions.

4. Conclusions

In summary, Fe-based oxide materials, Fe_2O_3, Fe_3O_4, and FeOOH, were synthesized by microwave–hydrothermal route at short reaction times of 15 min to 2 h. Cube-like Fe_2O_3, FeOOH nanorods and Fe_3O_4 particles were crystallized by controlling the hydrolysis and redox reactions of single $FeCl_3$ or $FeCl_2$ aqueous solutions at different reaction temperatures and reaction times. The Fe-based materials were tested for anodes and cathodes of lithium-ion battery and as supercapacitors electrode materials to study their potential electrochemical applications. The electrochemical results prove that FeOOH showed better anodes capacity as lithium-ion battery than that of Fe_2O_3 or Fe_3O_4. The microwave–hydrothermally synthesized Fe-based materials are promising lithium-ion battery anode materials.

Table 3
Specific capacitances of supercapacitors.

Sample no.	Specific capacitance (F/g) at current density of 1 A/g for potential window of 1.0 V
1	2
2	6 (1.2 V)
3	9
4	14
5	11

Acknowledgments

Financial support from the National Natural Science Foundation of China (Grant nos. 50872016, 20973033 and 51125009), the National Natural Science Foundation for Creative Research Group (Grant no. 21221061) and the Hundred Talents Program of the Chinese Academy of Sciences is acknowledged. Ms. Huang Wenyan gratefully acknowledges the financial sponsorship of Changzhou University Overseas Research and Training Program through an award. Dr. Ma Jianfeng gratefully acknowledges the financial sponsorship of Jiangsu Overseas Research and Training Program for University Prominent Young and Middle-aged Teachers and Presidents through an award.

References

[1] J. Liu, D. Xue, Thermal oxidation strategy towards porous metal oxide hollow architectures, Adv. Mater. 20 (2008) 2622.
[2] J. Liu, H. Xia, D. Xue, L. Lu, Double-shelled nanocapsules of V_2O_5-based composites as high-performance anode and cathode materials for Li ion batteries, J. Am. Chem. Soc. 131 (2009) 12086.
[3] F. Liu, S. Song, D. Xue, H. Zhang, Folded structured graphene paper for high performance electrode materials, Adv. Mater. 24 (2012) 1089.
[4] C. Sun, S. Song, D. Xue, H. Zhang, Crystallization of oxides as functional materials, Funct. Mater. Lett. 5 (2012) 1230002.
[5] S. Komarneni, R. Roy, Titania gel spheres by a new sol–gel process, Mater. Lett. 3 (1985) 165.
[6] S. Komarneni, R. Roy, Q.H. Li, Microwave–hydrothermal synthesis of ceramic powders, Mater. Res. Bull. 27 (1992) 1393.
[7] K. Chen, Y.D. Noh, K. Li, S. Komarneni, D. Xue, Microwave−hydrothermal crystallization of polymorphic MnO_2 for electrochemical energy storage, J. Phys. Chem. C 117 (2013) 10770.
[8] Y. Zhang, C. Sun, P. Lu, K. Li, S. Song, D. Xue, Crystallization design of MnO_2 towards better supercapacitance, Cryst. Eng. Comm. 14 (2012) 5892.
[9] K. Chen, D. Xue, Nanoscale surface engineering of cuprous oxide crystals: the function of chloride, Nanosci. Nanotechnol. Lett. 3 (2011) 383.
[10] Y. Zhang, C. Sun, D. Xue, A simple self-template strategy to synthesize ε-MnO_2 and its application in supercapacitors, Mater. Focus 1 (2012) 245.
[11] K. Li, Y. Li, D. Xue, Band gap engineering of crystal materials: band gap estimation of semiconductors via electronegativity, Funct. Mater. Lett. 5 (2012) 1260002.
[12] C. Sun, D. Xue, Calculation of structural characteristics of $Cd_{1-x}Ca_xO$ (x=0–1), Mater. Res. Innov. 17 (2013) 27.
[13] P. Yang, K. Li, D. Xue, Anisotropic hardness estimations of some inorganic functional materials, Funct. Mater. Lett. 5 (2012) 1250003.
[14] K. Li, J. Shao, D. Xue, Calculation of impurity energy levels of transition metal ions in inorganic crystals based on electronegativity, Mater. Res. Innov. 17 (2013) 218.
[15] K. Li, Y. Li, D. Xue, Band gap prediction of alloyed semiconductors, Funct. Mater. Lett. 4 (2011) 217.
[16] K. Chen, Y.D. Noh, S. Lin, S. Komarneni, D. Xue, Crystallization of MnO_2 by microwave–hydrothermal synthesis and its applications for supercapacitors and lithium-ion batteries, Mater. Focus 2 (2013) 86.
[17] Y. Zhang, D. Xue, Mild synthesis route to nanostructured alpha-MnO_2 as electrode materials for electrochemical energy storage, Funct. Mater. Lett. 5 (2012) 1250030.
[18] D. Cui, K. Gao, P. Lu, H. Yang, Y. Liu, D. Xue, Mild solution route to mixed-phase MnO_2 with enhanced electrochemical capacitance, Funct. Mater. Lett. 4 (2011) 57.
[19] K. Chen, A.C. Donahoe, Y.D. Noh, S. Komarneni, D. Xue, $LiMn_2O_4$ based materials as anodes for lithium-ion battery, Ceram. Int. http://dx.doi.org/10.1016/j.ceramint.2013.09.128, in press.
[20] K. Chen, S. Song, D. Xue, Hopper-like framework growth evolution in cubic system: a case study of Cu_2O, J. Appl. Crystallogr. (2013)http://dx.doi.org/10.1107/s0021889813022322.
[21] K. Chen, D. Xue, Chemoaffinity-mediated crystallization of Cu_2O: a reaction effect on crystal growth and anode property, Cryst. Eng. Comm. 15 (2013) 1739.
[22] K. Chen, D. Xue, pH-assisted crystallization of Cu_2O: chemical reactions control the evolution from nanowires to polyhedral, Cryst. Eng. Comm. 14 (2012) 8068.
[23] B. Dunn, H. Kamath, J.M. Tarascon, Electrical energy storage for the grid: a battery of choices, Science 334 (2011) 928.
[24] K. Li, J. Shao, D. Xue, Site selectivity in doped polyanion cathode materials for Li-ion batteries, Funct. Mater. Lett. 6 (2013) 1350043.
[25] S. Komarneni, W. Hu, Y.D. Noh, A. Van Orden, S. Feng, C. Wei, H. Pang, F. Gao, Q. Lu, H. Katsuki, Magnetite syntheses from room temperature to 150 °C with and without microwaves, Ceram. Int. 38 (2012) 2563.
[26] X. Lou, X. Wu, Y. Zhang, Goethite nanorods as anode electrode materials for rechargeable Li-ion batteries, Electrochem. Commun. 11 (2009) 1696.
[27] K. Chen, S. Song, D. Xue, Vapor-phase crystallization route to oxidized Cu foils in air as anode materials for lithium-ion batteries, Cryst. Eng. Comm. 15 (2013) 144.
[28] K. Chen, D. Xue, Chloride Assistant crystallization of Cu_2O polyhedron film by oxidation of copper foil in liquid phase, Mater. Focus 1 (2012) 203.